CONF-960482--6

WSRC-MS-95-0527

Simulation and Analysis of the Plutonium Shipping Container Subject to 30-Foot Drops (U)

by

C. Gong

Westinghouse Savannah River Company
Savannah River Site
Aiken, South Carolina 29808

N. K. Gupta

R. J. Gromada

A document prepared for 1996 SCS SIMULATION MULTICONFERENCE at New Orleans from 04/08/96 - 04/11/96.

DOE Contract No. DE-AC09-89SR18035

This paper was prepared in connection with work done under the above contract number with the U. S. Department of Energy. By acceptance of this paper, the publisher and/or recipient acknowledges the U. S. Government's right to retain a nonexclusive, royalty-free license in and to any copyright covering this paper, along with the right to reproduce and to authorize others to reproduce all or part of the copyrighted paper.

DISTRIBUTION OF THIS DOCUMENT IS UNLIMITED

MASTER

DISCLAIMER

This report was prepared as an account of work sponsored by an agency of the United States Government. Neither the United States Government nor any agency thereof, nor any of their employees, makes any warranty, express or implied, or assumes any legal liability or responsibility for the accuracy, completeness, or usefulness of any information, apparatus, product, or process disclosed, or represents that its use would not infringe privately owned rights. Reference herein to any specific commercial product, process, or service by trade name, trademark, manufacturer, or otherwise does not necessarily constitute or imply its endorsement, recommendation, or favoring by the United States Government or any agency thereof. The views and opinions of authors expressed herein do not necessarily state or reflect those of the United States Government or any agency thereof.

This report has been reproduced directly from the best available copy.

Available to DOE and DOE contractors from the Office of Scientific and Technical Information, P.O. Box 62, Oak Ridge, TN 37831; prices available from (615) 576-8401.

Available to the public from the National Technical Information Service, U.S. Department of Commerce, 5285 Port Royal Road, Springfield, VA 22161.

WSRC-MS-95-0527

SIMULATION AND ANALYSIS OF THE PLUTONIUM SHIPPING CONTAINER SUBJECT TO 30-FOOT DROPS

Chung Gong

Nick K. Gupta

Richard J. Gromada

Savannah River Technology Center
Westinghouse Savannah River Company
Aiken, South Carolina

Keywords: Applied mechanics, Numerical methods, Dynamics, Nonlinear plasticity.

ABSTRACT

The shipping container 5320 is a shipping package for radioactive materials. In order to maintain the component in this packaging within the sub-critical state when subjected to any kind of Hypothetical Accident Conditions (HAC), this Type B packaging is designed with various impact limiters. The present study is to examine the energy absorbing capacity of the impact limiter design of this container subjected to a 30-foot drop onto a flat unyielding horizontal surface in each of the three critical dropping orientations.

The 5320 packaging consists of a group of aluminum cylindrical shields and a steel base plate, the stainless steel primary and secondary containment vessels are enclosed in the shield tank system. The critical component is sealed in the primary containment vessel. On top of the shield tank a hemispherical shell is attached as an impact limiter. The overall geometry exhibits axial symmetry. However, the fins on the tank surface, the webs between inner and outer tank shells and the closure bolts deprive the container configuration of its symmetry.

This paper presents the results of a three dimensional nonlinear dynamic impact analysis. This analysis shows the deformed configuration of the container caused by the impact and also determines the effects of different stress wave paths in three distinct drops on the stress states in the critical component. The solution to the problem was obtained using the ABAQUS (explicit) finite element computer code. The nonlinearity of this analysis involves large structural deformation, elasto-plastic materials with strain hardening as well as multiple contact interfaces. Three drop orientations were studied, namely, top down impact, bottom down impact and side impact. Results will be compared against actual drop test data.

INTRODUCTION

The plutonium oxide shipping container is designed to protect its contents against the Normal Conditions of Transport (NCT) and Hypothetical Accident Conditions (HAC) with double containment. The casket is composed of primary and secondary containment vessels with a gasketed closure in the secondary containment vessel. The secondary containment vessel is enclosed in a finned shield tank filled with WEP neutron shielding material. An impact limiter (a hemispherical shell) and a thermal shield are provided on the top of the cask to protect the closure of the secondary containment vessel. Figure 1 is a sectional view of the shipping container 5320 showing its major components.

In order to analyze the effects of impact from 30-foot drops upon the integrity of the shipping container, a comprehensive dynamic simulation and analysis of the entire structure is helpful.

The container consists of seven different materials. The structural components assembled to protect the major content in the container are fabricated with various contact interfaces. The exterior symmetric configuration is lost through the bolt connection in the secondary containment vessel (EP-62) closure.

Considering the three distinct drop orientations, the asymmetric configuration and the multiple contact interfaces, the container can only be analyzed with three dimensional nonlinear finite element model.

The graphic code, PATRAN is used for modeling the geometry of the container. The nonlinear finite element analysis code, ABAQUS (Explicit) is utilized to carry out the calculations.

In this structure the cushioning material (honeycomb absorber) between the stainless steel components EP-61 (primary containment vessel) and EP-62 (secondary containment vessel) is comparatively insignificant. The outer container (the aluminum shield) plays a major role in the impact dynamics. A few important mechanical factors considered in this dynamic analysis are:

- Material nonlinearity, elastic-plastic responses.
- Geometric nonlinearity, large deformation and finite strains.
- Wave propagation through the entire structure.
- Discontinuities between the interfaces of several structural components.

PURPOSE AND SCOPE OF THE STUDY

Over more than a half century, the major technique in damage mitigation of packaged articles during transportation has been the use of the drop test. Due to lack of efficient computing device, dynamic impact analysis of a deformable mechanical system has been practically prohibitive. In 1945, Professor Raymond D. Mindlin of Columbia University wrote an extensive paper [Mindlin, 1945] on dynamics of package cushioning, which provides guidance in dynamic analysis of shipping containers.

In that paper, Mindlin idealized the package system by "lumping the parameters". For example, the outer container is considered as a single mass, the cushioning is considered as a massless spring with friction losses. The result of this idealization is to lose some of the fine detail of the real distributed system such as wave propagation through the cushioning and higher modes of vibration in the shipping container structure and in the packaged article.

The structure of the shipping container 5320 consists of more than 20 different structural components and seven different materials. Between the various structural components, there are at least six contact interfaces. The technique of "lumping the parameters" is inadequate in modeling this structural system.

The mathematical modeling and simulation of a physical system can serve many purposes, for instance:

- To search for optimized geometric configuration of the shipping container subjected to various physical conditions.
- To demonstrate and clarify some possible structurally weakness in the container subjected to various physical situations.
- To provide detail stress analysis for the components of the shipping container during the design process.
- To calibrate the strain gauges and accelerometers in a drop test.
- To analyze the impact intensity and paths to the packaged product during a hypothetical drop incident.

It is essential to understand the mechanical effects of interfacial arrangements between the structural components in the shipping container with respect to a certain applied loading. This analysis provides the impact and stress distribution as well as deformation configuration of the shipping container for three 30-foot drops along three axial directions. The results will be compared with the available drop test data.

Mechanically, this analysis will consider the following factors:

- Geometrically linear and non-linear deformations
- Materially elastic and inelastic behaviors
- Dynamic and impact loading conditions
- Kinematically continuous and discontinuous

DESCRIPTION OF THE PROBLEMS

Geometric Configuration

The overall appearance of the shipping container (cask) is an upright circular cylinder with a domed top, as shown in Figure 1. The main body of the cask consists of a shield tank, an impact limiter (top hat), a thermal shield and a base. The shield tank is composed of top plate, neutron shielding (water-extended polyester), webs, axial cooling fins, outer shell, inner shell, and bottom plate. The base includes a base plate, cage (personnel screen), and four casters. Inside the inner shell of the shield tank, a secondary containment vessel (EP-62) which consists of vessel body, flanged closure lid, closure bolts and an attachment bolt at bottom (to be bolted to the base plate) is press fitted. The primary containment vessel (EP-61) is installed inside the vessel body of the secondary containment vessel. The primary containment vessel consists of a vessel body, cap and plug. On both ends of the EP-61 there are stainless steel honeycomb spacers (energy absorbers). The product canister (EP-60) is inserted in the vessel body of EP-61.

Material

Except the neutron shielding (water-extended polyester (WEP)), the shield is made of aluminum. The bolts are made of high tension steels. The EP-60, EP-61 and EP-62 are all stainless steel confinement vessels. The top hat is fabricated from 304L stainless steel. The base plate is of carbon steel. The modulus of elasticity, Poisson's ratio and mass density for the Type 304L and Type 304 stainless steel are 28,300 ksi, 0.3 and 0.0007324 pound-sec^2/inch^4, respectively.

The mechanical properties of 304 and 304L grades were derived from the tensile tests on test coupons obtained from unirradiated 304 and 304L reactor components at Savannah River Site. These tests showed very little variation in the true stress and true strain values of these two grades of 304 stainless steel. Therefore, only one set of true stress true strain data is used for 304 and 304L in the analysis. Also the tensile properties of 316 grades are similar to the 304 grades. Based on these observations, it is concluded that the dynamic response of the 5320 package fabricated with 304L and 316L grades will be similar to the response of the package made with 304 and 316 grade.

The stress strain curve of the Type 316 stainless steel is digitized from a handbook [Structural Alloys, 1993]. The properties of the high strength steel for the bolts are obtained from a SAE handbook [SAE, 1992].

The mechanical properties of SB-241 Grade 6061-T6 Aluminum are taken from the metals handbook [ASM, 1990] and a report [Daugherty, 1991]. The true stress natural strain curve at room temperature (70° F) may be generated approximately by the formula:

$$True\ Stress = 57.8 * (Natural\ Strain)^{0.066}$$

The true stress natural strain curve for the ASTM A36 steel is converted from the data in [ASM, 1987].

The stainless steel honeycomb energy absorber has a crush strength of 1,500 psi. Initially the honeycomb under compression has a bare compressive strength which is much higher than the crush strength. By ignoring the bare compressive strength, the honeycomb material is modeled as an isotropic elastic-perfect plastic material. The modulus of elasticity of the stainless steel honeycomb is assumed to be in the order of one tenth of that of the solid stainless steel. To compensate the lower strength in the minor axes, the modulus of elasticity of the stainless steel honeycomb is chosen as 1,000 ksi and the Poisson's ratio to be 0.1. The yielding limit is 1.5 ksi.

No credit is taken for the energy absorbing capability of the water-extended polyester (WEP). The mass of the WEP is smeared over the surface of the aluminum webs. The structural and viscous damping properties of the structural components of the shipping cask are neglected in this analysis. This is conservative.

Type of Problems Considered

In this analysis, three loading conditions on the shipping container have been considered:

(1) Vertical upright (bottom) drop from 30-foot height
(2) Vertical upside-down (top) drop from 30-foot height
(3)Lateral (side) drop from 30-foot height

All the three drops are directly impact upon a flat unyielding surface.

METHOD OF ANALYSIS

Pre- and Post-processor

P3/PATRAN® [P3/PATRAN®, 1993] is a versatile geometric and graphic modeling code developed by PDA Engineering. The P3/PATRAN system's ability to interface with a large array of applications is provided by the PATRAN Neutral File, PATRAN Results File, and Application Interface. Post-processing of the results was accomplished using ABAQUS® POST.

Main Processor

ABAQUS® [ABAQUS®, 1993, Hibbitt et al, 1993] is a general purpose finite element analysis program with special emphasis on advanced linear and nonlinear structural engineering and heat transfer applications. Hibbitt, Karlsson & Sorensen, Inc. (HKS)

developed and support this computer code. The ABAQUS® version presently in use at SRS (5.4-1N) is marketed by HKS as a "Nuclear QA Grade" code that complies with the NQA-1 quality assurance standard. ABAQUS/Explicit is an explicit (integration) dynamics finite element program that reduces a great deal in matrix operations and consequently reduces the requirement of computer memory.

FINITE ELEMENT MODELS

The geometric configuration of the shipping container 5320 is essentially axially symmetric, however, the bolts in the EP-62 flanges and along the rim of the impact limiter (top hat) are not axially symmetric. Except in the case of internal pressure loading, the applied loading and boundary conditions are asymmetric. Ideally, the whole shipping container 5320 system can be modeled in three dimensional finite element mesh with various combinations of initial conditions and boundary conditions.

The dynamic impact loading during the postulated drop tests will inflict traumatic deformation to the shipping container 5320 system. The impact loading generates elastic and plastic waves in the shipping container 5320 system. In order that the finite element analysis can sufficiently simulate the stress waves at high frequencies (in the range of 500,000 hertz to 1,000,000 hertz), the finite element mesh must be sufficiently fine such that the distortion of the wave forms in the system will be within the tolerance [Gong, 1977].

Based upon preliminary analytical study, one universal finite element model is created for all the three problems. Since the whole shipping container 5320 system maintains a plane symmetry that is also compatible with the three orientations of drop, the container is modeled in half of the structure with a plane containing the vertical central axis of the shipping container as the plane of symmetry.

The purpose of this analysis is to examine the structural integrity of the shipping container 5320 subject to drop impact. Some container components which have little or no significant structural stiffness will not be included in the finite element model (the thermal shield, the water-extended polyester (WEP), axial cooling fins, and the casters). However, the mass of the WEP is added to the mass of the aluminum webs. The mass of the axial cooling fins is included in the mass density of the outer shell of the shield tank.

The product canister (EP-60) is well shock-protected in the vessel body of the primary containment vessel (EP-61). The dynamic effect of the EP-60 is dominantly a rigid body. To include the mass effect, the mass of the EP-60 is added to the mass of EP-61.

The interfaces between the structural components of the container system have various connectivity conditions. The characteristics of the interfaces will influence the dynamic behavior of the system. The mathematical models of the interfaces provide limited functions of the real structure. In all the interfaces, the friction effects are ignored, because there is no experimental data which can identify the nature of friction in the interfaces. Without the knowledge of the friction in those shrink-fitted interfaces, the best approximation in this analysis is making the interfaces connected.

According to the dynamic behavior of the structural system, the interface modeling of the shipping container is delineated as follows:

The vessel body of the EP-62 is shrink-fitted into the inner shell of the shield tank. The friction between the interface is not available. If the interface is connected, the increased stiffness will enhance the impact in EP-62 during drop. Therefore, the interface between EP-62 and the inner shell of the shield tank is connected.

The interface between the vessel bodies of EP-62 and EP-61 is completely open. The honeycomb spacers (energy absorber) remain attached to the EP-61 and EP-62 on both ends (not laterally). Comparatively the mechanical properties of the honeycomb are much weaker than the steels; there will be no significant mechanical effects on the analysis.

The base plate is detached from the bottom plate of the shield tank. However, the base plate is connected to the bottom of the EP-62 through the attachment bolt. A gap is left between the tip of the attachment bolt and the bolt cavity in the bottom of the EP-62.

The EP-62 closure lid flanges (top and bottom flanges) are not connected. The flange bolts through the bolt holes in the flanges are continuous and attached to the holes. The interface between the bottom surface of the EP-62 bottom closure flange and the top plate of the shield tank is a free sliding surface.

The rim of the impact limiter (top hat) and the top plate of the shield tank are joined only through the attachment bolts. The interface between the top hat rim and the top plate is separable but is not penetrable. Actually all the disconnected interfaces defined above are separable but are not penetrable. In terms of traction, these disconnected interfaces are either traction free or in compression during the time history of impact.

The initial condition of each of the three drops is an initial velocity of 527.5 inches per second at the moment when the container just touches the ground. In each of the attachment bolts, 4 ksi initial tension is applied. The unyielding ground in each case is simulated with a rigid surface in each location.

For the vertical upright (bottom) drop, the base plate is supported at the locations of the casters. The patches where the casters are located on the base plate are defined as contact pairs with the rigid ground surface at the same location as the base plate.

In the case of vertical up-side down (top) drop, the rigid ground surface is right at the top of the impact limiter (top hat). The contact pair is defined as the top hat and the rigid top surface.

A side rigid ground surface is modeled for the lateral (side) drop incident. Initially the edge of the base plate is in touch with the rigid surface and the rest of the container is still in the air. The top plate of the shield tank will drop on the rigid ground later. If the edge of the top plate would not bend in the drop, the top hat could not touch the rigid ground surface. Nevertheless, after the top plate edge touches the ground and bends at the edge, the kinetic energy in the container system has been enormously reduced. The secondary impact in the top hat will not significantly affect the impact in the EP-62 closure area as the results indicate.

The impact in a 30-foot drop will generate high mechanical oscillatory frequencies in the container system. For relatively soft components, such as the aluminum webs, stainless steel top hat, and steel base plate, the high frequency modes are mechanically insignificant. Whereas, the small (in size) attachment bolts are considerably stiff. The stresses in the bolts are susceptible to high order modes. The integrity of those attachment bolts is an essential concern in this analysis. Therefore sufficiently high frequency components should be included in this finite element analysis model. The range of frequencies in this model is from 0.0 (rigid body motion) to 500,000 hertz. The element size is a function of wave length and error tolerance [Gong, 1977].

In this analysis, three 30-foot drops in three different orientations are discussed. The impact induced waves will propagate, reflect and refract in all directions. To accommodate the finite element model to the possible impacts in all the directions, the finite element meshes are constructed as shown in Figure 2.

The container is modeled in solid continuum elements as well as structural shell elements. The EP-62 bottom cylinder, attachment bolt, closure lid flange and the bolts are discretized in solid elements. The EP-61 cap and plug and the energy absorbers at the top and bottom are also modeled in solid elements. The rest of the container system is meshed with structural shell elements. The mesh size distribution in the model reflects the potential wave propagation patterns.

The total number of elements is 14,381, and the total number of nodes is 15,416. In this model, besides the boundary conditions as described, the various interfacial conditions also require additional equations of constraint. The total number of variables which includes the degrees of freedom and the Lagrange multiplier variables is 64,533.

Based upon the elastic wave speed and element sizes in the finite element model of the container, ABAQUS automatically computes the time increment in the explicit dynamic analysis. This computed time increment will be maintained through the completion of the calculation.

The ABAQUS / Explicit has been installed on CRAY-SN9066. The lateral (side) drop and both the vertical (upright "bottom" and upside down "top") drops were run on CRAY-SN9066. Each of the three calculations took approximately 84 CPU hours for 15 milliseconds of analysis. The time increment used in all the three drops is 0.06939 microseconds. The total number of time increments in the 15 milliseconds calculation is 216,184. The time history of stresses, accelerations and velocities during the drop impact is saved in the interval of every 15 microseconds (total 1006 data points). The dynamic responses of the container are saved only for a limited number of elements and nodal points. The vectorial velocity and acceleration time histories are kept for 72 nodal points. The tensorial stress and von Mises equivalent stress are saved for 119 elements.

RESULTS

In each of the three drop analyses, the initial kinetic energy in the container system is

K.E.= one half of the container mass times velocity square

$$= 0.5 * 0.4318 * (527.5)^2 = 60{,}076 \text{ inch-pounds.}$$

In this formula, 0.4318 lbs-sec^2 / in is the total mass of the container in the finite element model which utilizing the plane symmetry of the kinematics, consists of only half of the container. The time variation of the kinetic energy elucidates the global mechanical behavior of the container system. The variation of kinetic energy after 15 milliseconds is relatively insignificant. Hence the time histories of the kinetic energy of the three drop calculations are plotted up to 15 milliseconds as shown Figure 3.

The time history of kinetic energy in the container tells the overall motion of the system during the drop. The time dependent stress distribution in the container is a function of the elastic and plastic waves propagating in the system.

(1) Vertical upright (bottom) drop

As the bottom of the base plate touches the ground the kinetic energy sharply reduces due to the plastic dissipation in the base plate. The plastic deformation in the base plate is comparatively small. As the impact generated waves travel upward, the impulse gradually slacken the downward velocity of the system. The wave speed varies in magnitude from component to component as a function of mechanical properties and deformation of the particular structural member. The speed of wave propagation is in the order of a few hundred times of the initial velocity. Before the container rebounds from the ground, mechanical (elastic and/or plastic) waves may have traveled through the cask more than 5 times. During this period the kinetic energy decreases almost linearly, until the moment when the system is approaching rebounding at 0.61506 milliseconds, the rate of decline of kinetic energy starts slowing down. Most of the kinetic energy is dissipated in plastic deformation of the structure; the rest is stored as recoverable elastic strain energy. In the real physical situation the kinetic energy may be dissipated into heat and other forms of energy in addition to elastic strain energy and plastic deformation.

At 0.6454 milliseconds since the bottom of the container touched the ground, the kinetic energy in the system reaches the minimum of 3,306 inch-pounds. Meanwhile the elastic strain energy in the system overcomes the downward motion and the whole container starts to rebound. From the time the base plate touched the ground to 0.6454 milliseconds, the bottom of the container remains on the ground. The mechanical waves generated by the impact propagate upward. The upward impulse is in conflict with the downward momentum from the dropping. Figure 3 compares the time histories of the kinetic energy during the three drops. Within the first millisecond most of the kinetic energy is dissipated through plastic deformation. A part of the kinetic energy is stored as recoverable elastic strain energy. The kinetic energy reaches the minimum when most of the container system starts to reverse the orientation of the velocity. Right before the bottom plate leaves the ground the kinetic energy increases as the stored strain energy releases its power. As waves propagate in the container in this period, more energy is dissipated through plastic deformation. After 2 milliseconds the energy dissipation in the system is negligible, while the elastic strain energy maintains steady wave propagations in the container.

At the bottom of the container where the drop impact engages directly, the mechanical responses (acceleration and stresses) rise instantaneously and drastically. The maximum responses in the bottom region are at the beginning of the impact and just before the rebound of the container.

The maximum von Mises stress in this bottom drop occurs in the knuckle of the EP-62 bottom closure cap at approximately 1.755 milliseconds. The maximum von Mises stress is 51.562 ksi. The von Mises stress in the elements at the junction of the closure cap and the EP-62 cylinder has a maximum value of 44.77 ksi in element 4528 at 1.785 milliseconds. The bottom of the EP-62 is closer to the direct impact region. To compare the time history of von Mises stress in an element at the bottom of the EP-62 with that in the top elements will elucidate the characteristic of the waves propagating in the container. The von Mises stress in a bottom element (4538) has a maximum of 40.468 ksi at 1.59 milliseconds. The magnitude of the maximum stress increases as the location of the stressed element moves upward and away from the direct impact area. After the von Mises stress reached its peak, the stress fluctuation are slowing down in the upper elements while the stress in the bottom edge element still oscillates widely. The von Mises in the bottom edge element has a mean value of 15 ksi. The stress in the top edge element varies about 12 ksi. The element in the bottom closure cap has little residual stress. The elastic limit of the 304 stainless steel is 37.84 ksi. The elements in all the three regions mentioned above are plastically deformed in the first couple milliseconds.

As the time history of the energies shown that the most of the kinetic energy is dissipated in plastic deformation in the first two milliseconds, A small amount of the kinetic energy is stored as elastic strain energy. During the first two milliseconds, waves

propagate from the bottom of the EP-62 up to the top. The impact waves in the closure area cause high bending stress in the lower closure cap. The relatively confined configuration in the EP-62 and shield tank connection, causes stress intensification in the structural components due to multiple wave reflections.

The EP-62 closure flanges are tied together with bolts. The interface of the two flanges can carry only compressive pressure. During the wave propagations the interface can transmit compressive stress but not tensile and/or shear stresses. This tension free interface increases the compressive stress in the components in this area.

After the container rebounds from the rigid ground, the whole system vibrates with the propagation of elastic waves. The existing of a tension (and shear) free interface exhibits in the time history of von Mises stress in the EP-62 (bottom) closure cap. The pattern of the elastic response indicates that the stress is intensified when the wave is in compression. The stress in the closure cap diminishes as tension wave passes the element. A few elements away from the middle of the closure cap, the semicontinuous interface has little or no influence to the top edge elements in the EP-62.

For a rigid body approximation the acceleration at the centroid of a structure may be used to estimate the possible stress in the structural components. However, in a deformable body with geometric and material nonlinearities, the characteristics of wave propagations and inter-component constraints will determine the stress distribution in the structural system. The acceleration is an indicator of the intensity of the dynamic impact in a specific location. Without additional physical data the magnitude of acceleration alone may not provide any stress state information.

The acceleration at the top of the EP-61 is 1.049E+06 inches per second per second or 2,717 *g* (gravitational acceleration).

(2) Vertical up-side down (top) drop

The impact limiter (top hat) hits the ground at the apex. The stress concentration in the apex area immediately spreads to the entire top surface. The impact has a tendency to buckle the top hat wall. Initially the impact force deflects the shallow shell of the top hat and the rate of energy dissipation is low. As the deformation of the apex propagates to the surrounding cylindrical wall, the top drop inflicts more dynamic impact on the container. The area of plastic deformation increases and the rate of energy dissipation steadily grows until the system gradually reverses the direction of the vertical velocity. The kinetic energy in the container reaches its minimum of 28.92 inch-pounds at 4.56 milliseconds. In the meantime the plastic dissipation stops and the stored elastic strain energy provides strength for the rebound of the container.

The dynamic responses of the container system are considerably weaker than those in the bottom drop case. This demonstrates that the impact limiter (top hat) is quite effective and it serves the purpose.

Under direct impact the von Mises stress at the apex of the top hat reached 81.96 ksi just before the container started rebounding. The primary and secondary containment vessels are well protected from dynamic impact by the impact limiter. The maximum von Mises stress in the bottom closure cap is 38.73 ksi. The stress at the top edge of EP-62 is slightly lower at 38.05 ksi which is close to the elastic limit, 37.84 ksi. The maximum acceleration in the EP-61 top is 390,800 inches/sec^2, or 1,012 *g*.

(3) Lateral (side) drop

Laterally the edges of the protruding structural components of the container are not lined up along a straight line that is parallel to the central axis. Consequently, as the container is being dropped with the central axis in a horizontal position, there will be at least three consecutive impact contacts of the container upon the ground.

Initially only the edge of the base plate touches the ground. The impact is transmitted to the container through the attachment bolt. The base plate is severely deformed at the bolt connection. The plastic deformation in the base plate and in the container dissipates energy. The kinetic energy is reduced. After an initial sharp growth, the rate of energy dissipation slows down until the edge of the top plate on the shield tank hits the ground at 1.71 milliseconds. The impact at the bottom plate gives rise to a moment about the centroid of the container. The angular acceleration caused by the moment increases the velocity at the edge of the top plate. This results in a slight rise in kinetic energy at the impact of the top plate.

The top plate is made of aluminum that is softer than the steels in the other components of the container. The edge of the top plate in contact is badly smashed during the impact. The energy dissipation in this period increases almost linearly.

As the edge of the top plate bends, the side surface of the impact limiter (top hat) touches the ground. At this moment (about 4.1 milliseconds) the strength of the impact diminishes significantly. While the dynamic collision dissipates much more energy, it also stores more elastic strain energy in the system. The three consecutive impacts generate elastic as well as plastic waves in the container. Before the container fully rebounds from the ground at 5.5201 milliseconds, the container experienced fluttering. The increase of kinetic energy in the period from 5.5201 milliseconds to 6.4501 milliseconds indicates that the container hits the ground again. The motion of the container combines rotational and linear displacements. The elastic strain energy stored in the system reaches the extreme at 5.31 milliseconds when the container starts to rebound. As the stored elastic strain energy plunges to a relative minimum at 6.495 milliseconds, the container is on the ground and deforms more elastically. The container will vibrate more before it finally rests on the ground.

The maximum von Mises stress in the neck of the EP-62 is 64.43 ksi which is well above the yield limit, 37.84 ksi. The von Mises stress in the EP-62 closure is 44.91 ksi. The bottom of EP-62 has a maximum stress of 39.51 ksi. In the primary containment vessel, EP-61, the top edge has a maximum von Mises stress of 47.28 ksi. It shows that the impact from the side drop is considerably severe. The plastic deformation of the containment vessels is also observed in the drop tests.

In all three calculations dynamic impact and plastic as well as elastic wave propagations are major concerns. The results of the three calculations are saved in ABAQUS output files. The tables at the end of this paper show the accelerations and stress intensities in the primary and secondary containment vessels.

CONCLUSION

The shipping container consists of structural components with various configurations and mechanical properties. Between the structural components the mechanical connectivity varies widely. There are gaps and tension free interfaces. The mass distribution in the system is considerably inhomogeneous. The wave propagations (from the drop impacts) in such a complex medium will generate stresses and accelerations over a very broad spectrum in space and time.

A comprehensive study of the results through processing of the output data is indispensable for the understanding of the dynamic behavior of the container. The waves generated in the dynamic impact propagate at various speeds in all the directions. The reflection, diffraction and refraction of waves at the structural and material discontinuities will produce stress and strain concentrations. High stresses may accumulate at a location far from the direct impact area and at a time after the initial collision. In general, the main product kept in the primary containment vessel insider the container is well protected in all the three drops.

REFERENCES

ABAQUS® (version 5.4-1N), 1993, is a registered trademark of a finite element analysis computer code developed by Hibbitt, Karlsson & Sorensen, Inc., 1080 Main Street, Pawtucket, Rhode Island 02860.

ASM, 1987, *"Atlas of Stress Strain Curves"*, p. 186 AMERICAN SOCIETY FOR METAL (ASM) INTERNATIONAL Handbook Committee-10th ed., Materials Park, OH 44073.

ASM, 1990, *"Metal Handbook"*, tenth edition, volume 2, pp. 62~122 (*102*), AMERICAN SOCIETY FOR METAL (ASM) INTERNATIONAL Handbook Committee-10th ed., Materials Park, OH 44073.

Daugherty, W. L., 1991, "Material Properties of Aluminum Alloys 1100, 6061, and 6063 (U)", SRL-EDG-91-0074, Westinghouse Savannah River Company, Aiken, SC.

Gong, C., 1977, "Dispersion and Anisotropy Induced in Finite Element Analysis," a paper presented at *Fourth International Conference on Structural Mechanics in Reactor Technology*, San Francisco, CA, U.S.A. August 15-19, 1977.

Hibbitt, Karlsson & Sorensen, Inc., 1993, *"ABAQUS Theory Manual,"* version 5.4.

Mindlin, R. D., 1945, "Dynamics of Package Cushioning", in *Bell System Technical Journal*, volume 24, 353-461.

P3/PATRAN® (version 1.2), 1993, is a registered trademark of PDA Engineering, Software Production Division, 2975 Redhill Avenue, Costa Mesa, California 92626.

SAE Handbook, 1992, Volume 1, Section 4.01, Society of Automotive Engineers, Inc., Warrendale, PA 15096.

Structural Alloys Handbook, Edition 1993, Volume 2, CINDAS-Purdue University, West Lafayette, IN, 47906.

ACKNOWLEDGMENT

The authors would like to thank Jeffrey W. Jerrell for his help in the modeling process using PATRAN.

The information contained in this article was developed during the course of work under Contract No. DE-AC09-89SR18035 with the U. S. Department of Energy. By acceptance of this paper, the publisher and/or recipient acknowledges the U. S. Government's right to retain a non-exclusive, royalty-free license in and to any copyright covering this paper along with the right to reproduce, and to authorize others to reproduce all or part of the copyrighted paper.

MAXIMUM ACCELERATIONS AT THE TOP OF EP-61 (NODE 11556)

DROP ORIENTATION	ACCELERATION (inches/second/second)	ACCELERATION (gravitational acceleration)
BOTTOM	1.049E+06	2,717
TOP	3.908E+05	1,012
SIDE	1.066 E+06	2,761

MAXIMUM STRESS INTENSITY IN EP-61

DROP ORIENTATION	TOP (ksi)	MIDDLE (ksi)	BOTTOM (ksi)
BOTTOM	15.91	13.92	9.072
TOP	6.01	4.69	7.65
SIDE	10.39	8.14	7.84

MAXIMUM STRESS INTENSITY IN EP-62

DROP ORIENTATION	TOP (ksi)	MIDDLE (ksi)	BOTTOM (ksi)
BOTTOM	44.17	26.97	32.14
TOP	42.39	9.09	10.29
SIDE	49.91	17.75	14.05

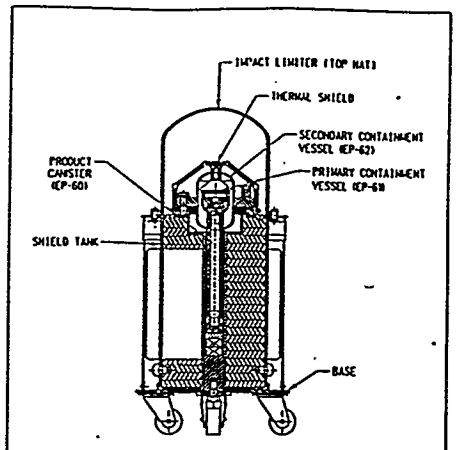

Figure 1. Shipping Container 5320 Assembly

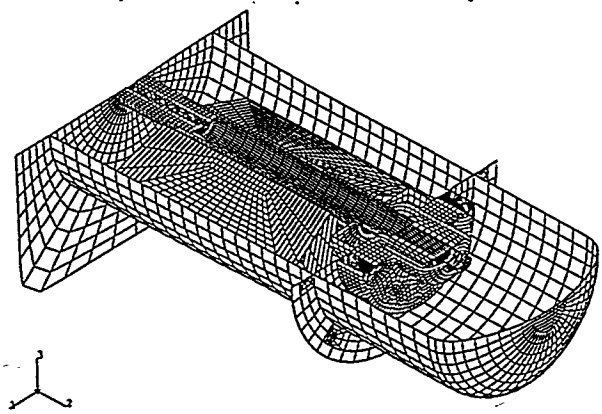

Figure 2. The Finite Element Mesh of the Shipping Container 5320

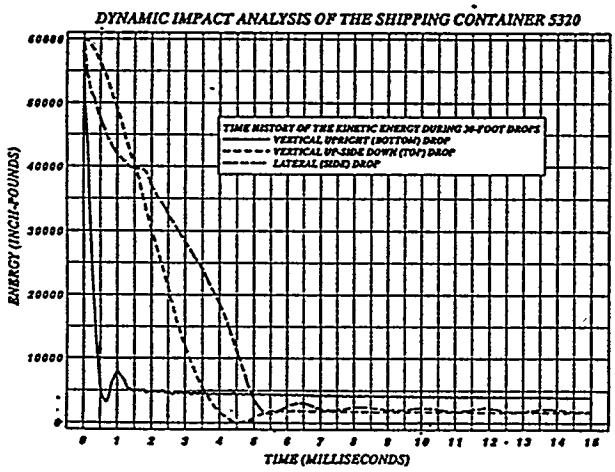

Figure 3. Time History of Total Kinetic Energy in the Container during each of the Three Drops

WESTINGHOUSE SAVANNAH RIVER COMPANY

INTER-OFFICE MEMORANDUM

Reference

NRTSC Technology On Time On Target

SRL-EDG-910074
Task 91-001-1
Subtask 3

March 21, 1991

To: J. K. Thomas, 773-41A

From: W. L. Daugherty, 773-41A

Technical Review: M. J. Morgan 4/2/91
M. J. Morgan Date

Subject: **Material Properties for Aluminum Alloys 1100, 6061 and 6063**

This memorandum transmits material property data for use in analysis of components fabricated from alloy 1100, 6061 or 6063 in the gamma heating scenario that is postulated to follow a hypothetical loss of cooling accident.

Due to a lack of high temperature data for alloy 6063, it is recommended for the present time that the properties for 6061 be applied to 6063. While differences exist between the two alloys that will lead to different properties, once irradiated to saturation levels, the resulting strengthening mechanisms are expected to dominate in either alloy and lead to similar properties. Specific alloys for alloy 6063 will be developed later if necessary.

Properties are provided for both irradiated and unirradiated material. The safety rod is out of the core during operation and therefore is essentially unirradiated. Other aluminum components may be irradiated or not depending on when the accident occurs during the life of the component.

Table 1 provides the following properties as a function of temperature, which are applicable to each of the aluminum alloys:

- Poisson's ratio
- Average coefficient of thermal expansion
- Young's modulus

Tables 2 through 5 provide tensile data for each alloy, unirradiated and irradiated, as a function of temperature, consisting of:

- Yield strength and corresponding true stress
- Ultimate tensile strength and corresponding true stress
- Engineering strain at max. load and corresponding true strain
- Total engineering strain and corresponding true strain
- Specific data points to define a true stress-true strain curve

Values for each of these properties are provided for a broad range of temperatures. For temperatures between those at which values are given, linear interpolation is appropriate to find the corresponding value.

Also provided in Tables 1 through 7 are notes describing the source/basis for the values given. The raw data from which the values are derived are found in the attached data sheets. Where more than one source was available for a given parameter at a given temperature, the average values are considered. However, more weight is given to sources that include trends with temperature and/or surveys of literature data that report average values from other researchers. Where particular weight is given to one or more sources, this is identified in the notes.

The tensile properties given in Tables 2 through 5 are used to develop true stress-true strain curves. These are developed by fitting a power law relationship to the available data points (at yield and UTS). Since the power law equation contains two unknowns (K and n), these two data points are sufficient to define a unique curve. These curves are shown in Figures 1 through 4. Each curve is extended to the true strain at failure.

It should be noted that tensile properties can display variation between different heats, and even between different specimens within the same heat. Therefore, the data presented in this memo are generally nominal values. Actual component behavior may vary depending on a number of factors. Accordingly, if the structural analysis shows that any sort of failure condition is approached, a reevaluation of material properties would be prudent. In particular, these aluminum alloys generally have little strain hardening and ductility can vary considerably, depending on specific conditions. Further, it may be inappropriate to extend the stress - strain curves beyond the point of maximum load, depending on the local stress state in the component. Therefore, if calculations show that the total strain exceeds the strain at maximum load, these curves may need to be reassessed.

Relatively little data exists at temperatures above 800 F. At about 600 to 800 F, differences between the alloys start to disappear. Irradiation effects also begin to anneal out in this temperature range. Both these effects depend on the time-temperature history. Therefore, if a component spends much time (greater than 1 hour) in this temperature range, the properties should be reassessed. If a component temperature reaches as high as 1000 F for any period of time, but does not reach the melting point, the properties should also be reassessed.

Attachment

cc: G. E. Mertz, 773-41A *
P. S. Lam, 773-41A *
R. L. Sindelar, 773-41A *
N. Kumar, 773-41A *
M. J. Morgan, 773-A *
Task 91-001-1 file, subtask 3

* without attachment

Table 1. Aluminum Alloy 1100 and 6061 Properties

Temperature (F)	Poisson's Ratio	Temperature coef. (x E-6 /F) *	Young's modulus (ksi)
70	(a) 0.33		(f) 10000
212			(g) 9530
400		(c) 13.5	(h) 8900
500			(h) 8100
600		(d) 14.3	(i) 6700
700	(b) 0.33		(j) 6300
800	(b) 0.34		(k) 5900
900	(b) 0.35		(k) 5400
1000	(b) 0.35		(k) 4900
1100	(b) 0.325		(k) 4200
1220		(e) 15.9 **	

* Average value from 70 F to given temperature.
** Upon melting, the vol. exp. is 0.073. As a liquid, the avg. temp. coef. from 1220 to 1340 F is 23.4 E-6 /F.
(...) - Letters refer to notes on the next page describing the source of each property.

$\alpha \Delta T \times L =$ [illegible]

Source Notes for Table 1 Properties:

(a) Data Sheet 1 Entry 4 (DS 1 E 4)
(b) DS 13 E 4
(c) DS 5 E 3 and DS 13 E 5
(d) DS 13 E 5 and DS 17 E 6 (to 620 F) average
(e) DS 17 E 6
(f) DS 5 E 5, DS 3 E 1, and DS 12 E 6
(g) DS 5 E 6
(h) DS 5 E 6, DS 3 E 1 , and DS 12 E 2 average
(i) DS 12 E 2 and DS 12 E 6 average
(j) linear interpolation
(k) Ratio of DS 13 E 1 value at 600 F to the 600 F value above (ratio = 0.684) was applied to the 800 - 1100 F values of DS 13 E 1

Table 2. Unirradiated Al 1100 Properties

Temp. (F)	Young's Mod. (ksi)	Yield Stress (ksi) Eng.	TRUE	Stress at Max. Load (ksi) Eng. (UTS)	TRUE	Strain at Max. Load Eng.	TRUE	True Strain at Failure	Power Law (s = K e^n) ** K	n
		(a)	(b)		(h)		(k)		(q)	(q)
70	10000	5	5.0	(c) 12.5	16.6	(i) 0.33	0.28	(l) 0.37	21.0	0.189
212	9530	5	5.0	(d) 11	13.9	(j) 0.26	0.23	(m) 0.37	17.7	0.167
400	8900	3.5	3.5	(e) 5	5.8	(j) 0.17	0.15	(n) 0.44	6.8	0.085
500	8100	2	2.0	(f) 3.5	3.9	(j) 0.12	0.12	(o) 0.5	5.0	0.110
600	6700	1.5	1.5	(d) 2.5	2.7	(j) 0.08	0.08	(o) 0.52	3.5	0.101
700	6300	1	1.0	(d) 2	2.1	(j) 0.07	0.06	(o) 0.54	3.0	0.126
800	5900	1	1.0	(g) 1.5	1.6	(j) 0.08	0.08	(p) 0.59	2.0	0.079

* Average value from 70 F to given temperature.

** This correlation uses true stress and true strain.

(...) - Letters refer to notes on the next page describing the source of each property.

True Stress - True Strain Curve data: *

70 F Strain	70 F Stress (ksi)	212 F Strain	212 F Stress (ksi)	400 F Strain	400 F Stress (ksi)	600 F Strain	600 F Stress (ksi)	800 F Strain	800 F Stress (ksi)
0	0	0	0	0	0	0	0	0	0
0.0005	5	0.0005	5	0.0004	3.5	0.0002	1.5	0.0002	1
0.02	10.0	0.02	9.2	0.02	4.9	0.02	2.4	0.02	1.5
0.05	11.9	0.05	10.7	0.05	5.3	0.05	2.6	0.05	1.6
0.10	13.6	0.10	12.1	0.10	5.6	0.10	2.8	0.10	1.7
0.20	15.5	0.20	13.5	0.20	6.0	0.20	3.0	0.20	1.7
0.30	16.8	0.30	14.5	0.30	6.2	0.30	3.1	0.30	1.8
0.37	17.4	0.37	15.0	0.40	6.3	0.40	3.2	0.45	1.9
				0.44	6.4	0.52	3.3	0.59	1.9
(r)	(r)	(r)	(r)	(r)	(r)	(r)	(r)	(r)	(r)

* For temperatures in between those given, use linear interpolation.

Source Notes for Table 2 Properties:

(a) Data Sheet 17 Entry 4 (DS 17 E 4) Table 2 (DS 17 E 2, E 4, & E 5, and DS 7 E 8 all represent the same data base). DS 7 E 5 values are in agreement

(b) Calculated from eng. value: $\sigma = s_y * (1 + s_y/E)$

(c) DS 17 E 4 Table 2, DS 17 E 5, and DS 7 E 4 average

(d) DS 17 E 4 Table 2

(e) DS 17 E 4 Table 2, DS 17 E 5, and DS 5 E 8 average

(f) DS 17 E 4 Table 2, DS 7 E 4, and DS 5 E 8 average

(g) DS 17 E 2 Figure 8

(h) Calculated from eng. value: $\sigma = s_{UTS} * (1 + e_{UTS})$

(i) DS 17 E 2 Figure 8 and DS 17 E 5 average

(j) DS 17 E 2 Figure 8 values reduced by 18%, corresponding to the average reduction of the 70 and 400 F values due to averaging with DS 17 E 5

(k) Calculated from eng. value: $\varepsilon = \ln(1 + e)$

(l) DS 17 E 2 Figure 4, DS 17 E 2 Figure 8, DS 17 E 5, and DS 7 E 6 average, converted to true strain

(m) Same as 70 F value, based on DS 17 E 2 Figure 4 and DS 17 E 2 Figure 8 trends

(n) DS 17 E 2 Figure 4, DS 17 E 2 Figure 8, and DS 17 E 5 average, converted to true strain

(o) DS 17 E 2 Figure 4, DS 17 E 2 Figure 8, and DS 7 E 6 average, converted to true strain

(p) Extrapolated on the basis of trend in DS 17 E 2 Figure 8

(q) Values from fit to true yield stress and true stress at max. load, with corresponding true strains

(r) First two values define elastic range; remaining values define plastic range, up to failure strain

Table 3. Irradiated Al 1100 Properties

Temp. (F)	Young's Mod. (ksi)	Yield Stress (ksi) Eng.	Yield Stress (ksi) TRUE	Stress at Max. Load (ksi) Eng. (UTS)	Stress at Max. Load (ksi) TRUE	Strain at Max. Load Eng.	Strain at Max. Load TRUE	True Strain at Failure	Power Law (s = K c^n) ** K	Power Law (s = K c^n) ** n
		(a)	(b)	(a)	(c)	(a)	(d)	(e)	(f)	(f)
70	10000	22.6	22.7	26.1	28.3	0.09	0.08	0.235	33.1	0.062
212	9530	19.1	19.1	21.7	23.2	0.07	0.07	0.175	26.9	0.055
400	8900	14.8	14.8	15.9	16.4	0.03	0.03	0.057	18.5	0.035
500	8100	10.4	10.4	11.2	11.5	0.03	0.03	0.054	12.9	0.033
600	6700	6.6	6.6	7.1	7.3	0.04	0.03	0.102	8.1	0.030
700	6300	4.1	4.1	4.4	4.6	0.04	0.04	0.086	5.0	0.026

* Average value from 70 F to given temperature.

** This correlation uses true stress and true strain.

(...) - Letters refer to notes on the next page describing the source of each property.

True Stress - True Strain Curve data: *

70 F Strain	70 F Stress (ksi)	212 F Strain	212 F Stress (ksi)	400 F Strain	400 F Stress (ksi)	600 F Strain	600 F Stress (ksi)	700 F Strain	700 F Stress (ksi)
0	0	0	0	0	0	0	0	0	0
0.0023	22.7	0.0020	19.1	0.0017	14.8	0.0010	6.6	0.0007	4.1
0.02	26.0	0.02	21.7	0.02	16.1	0.02	7.2	0.02	4.5
0.05	27.5	0.05	22.8	0.04	16.5	0.04	7.4	0.04	4.6
0.10	28.7	0.10	23.7	0.06	16.7	0.07	7.5	0.06	4.6
0.20	30.0	0.18	24.5			0.10	7.6	0.08	4.7
0.24	30.3								
(g)	(g)	(g)	(g)	(g)	(g)	(g)	(g)	(g)	(g)

* For temperatures in between those given, use linear interpolation.

Source Notes for Table 3 Properties:

(a) Data Sheet 17 Entry 4 (DS 17 E 4) Table 2 (DS 17 E 2, E 4, & E 5, and DS 7 E 8 all represent the same data base)

(b) Calculated from eng. value: $\sigma = s_y * (1 + s_y/E)$

(c) Calculated from eng. value: $\sigma = s_{UTS} * (1 + e_{UTS})$

(d) Calculated from eng. value: $\varepsilon = \ln(1 + e)$

(e) DS 17 E 4 Table 2, converted to true strain

(f) Values from fit to true yield stress and true stress at max. load, with corresponding true strains

(g) First two values define elastic range; remaining values define plastic range, up to failure strain

Table 4. Unirradiated Al 6061 Properties

Temp. (F)	Young's Mod. (ksi)	Yield Stress (ksi) Eng.		TRUE	Stress at Max. Load (ksi) Eng. (UTS)		TRUE	Strain at Max. Load Eng.		TRUE	True Strain at Failure		Power Law (s = K e^n) ** K	n
				(f)			(m)			(q)			(v)	(v)
70	10000	(a)	40	40.2	(g)	45	49.5	(n)	0.1	0.10	(r)	0.157	57.8	0.066
212	9530	(b)	40	40.2	(h)	41	44.3	(o)	0.08	0.08	(s)	0.166	48.3	0.033
400	8900	(b)	31	31.1	(i)	32	33.6	(o)	0.05	0.05	(s)	0.174	36.7	0.029
500	8100	(c)	21	21.1	(j)	22	22.8	(n)	0.04	0.04	(t)	0.166	25.2	0.030
600	6700	(d)	10	10.0	(j)	11	11.3	(n)	0.02	0.02	(t)	0.247	13.2	0.042
700	6300	(d)	6	6.0	(j)	6.5	6.6	(n)	0.02	0.02	(t)	0.315	7.5	0.032
800	5900	(d)	2.4	2.4	(k)	3.7	3.8	(n)	0.02	0.02	(u)	0.588	5.8	0.112
900	5400	(e)	1.6	1.6	(l)	2.2	2.2	(p)	0.02	0.02	(u)	0.588	3.1	0.080
1000	4900	(e)	1.2	1.2	(l)	1.6	1.6	(p)	0.02	0.02	(u)	0.501	2.1	0.070

* Average value from 70 F to given temperature.

** This correlation uses true stress and true strain.

(...) - Letters refer to notes on the next page describing the source of each property.

True Stress - True Strain Curve data: *

70 F		212 F		400 F		600 F		800 F		1000 F	
Strain	Stress (ksi)	Strain	Stress (ksi)	Strain	Stress (ksi)	Strain	Stress (ksi)	Strain	Stress (ksi)	Strain	Stress (ksi)
0	0	0	0	0	0	0	0	0	0	0	0
0.0040	40	0.0042	40	0.0035	31	0.0015	10	0.0004	2.4	0.0002	1.2
0.02	44.6	0.02	42.4	0.02	32.8	0.02	11.2	0.02	3.7	0.02	1.6
0.05	47.4	0.05	43.7	0.05	33.6	0.05	11.6	0.05	4.1	0.05	1.7
0.10	49.6	0.10	44.7	0.10	34.3	0.10	12.0	0.10	4.5	0.10	1.8
0.16	51.1	0.17	45.5	0.17	34.8	0.20	12.3	0.20	4.8	0.20	1.9
						0.25	12.4	0.30	5.0	0.30	2.0
								0.45	5.3	0.40	2.0
								0.59	5.4	0.50	2.0
(w)	(w)	(w)	(w)	(w)	(w)	(w)	(w)	(w)	(w)	(w)	(w)

* For temperatures in between those given, use linear interpolation.

Source Notes for Table 4 Properties:

(a) Data Sheet 12 Entry 4 (DS 12 E 4): this value also matches the average value for 212 F, consistent with Al 1100 trend
(b) DS 12 E 4, DS 12 E 1, and DS 14 E 3 Figure 4 average
(c) DS 12 E 4, DS 12 E 1, and DS 12 E 7 average
(d) DS 12 E 4, DS 12 E 1, and DS 12 E 7 average, biased toward DS 12 E 4, since that is the more complete data set
(e) DS 12 E 4: the DS 12 E 7 value is similar at 900 F

(f) Calculated from eng. value: $\sigma = s_y * (1 + s_y/E)$
(g) DS 12 E 3 and DS 14 E 2 Table 10
(h) DS 12 E 3, DS 14 E 2 Table 10, and DS 3 E 7 average: DS 14 E 3 Figure 4 value is a relative outlier and was ignored
(i) DS 12 E 3, DS 14 E 3 Figure 4, and DS 3 E 7 average: and DS 14 E 2 Table 10 and DS 3 E 4 values are relative outliers (especially compared to higher temp. data) and were ignored
(j) DS 12 E 3, and DS 3 E 7 average: and DS 14 E 2 Table 10 and DS 3 E 4 values are relative outliers (especially compared to higher temp. data) and were ignored
(k) DS 12 E 3, and DS 3 E 7 average
(l) DS 12 E 3

(m) Calculated from eng. value: $\sigma = s_{UTS} * (1 + e_{UTS})$
(n) At 212 and 400 F, average ratio of value for Al 6061 to corresponding value for Al 1100 is 3.3: this ratio was applies to Al 1100 values at other temperatures.
(o) DS 14 E 3 Figure 4
(p) Value at 800 F (0.024) is conservatively extrapolated as 0.02

(q) Calculated from eng. value: $\varepsilon = \ln(1 + e)$
(r) DS 12 E 5, DS 3 E 6, and DS 14 E 2 Table 10 average, converted to true strain
(s) DS 12 E 5, DS 3 E 6, DS 14 E 3 Figure 4, and DS 14 E 2 Table 10 average, converted to true strain
(t) DS 12 E 5 and DS 3 E 6, converted to true strain (DS 14 E 2 Table 10 values are outliers, probably due to long hold times at temperature)
(u) DS 12 E 5
(v) Values from fit to true yield stress and true stress at max. load, with corresponding true strains
(w) First two values define elastic range; remaining values define plastic range, up to failure strain

Table 5. Irradiated Al 6061 Properties

Temp. (F)	Young's Mod. (ksi)	Yield Stress (ksi) Eng.		TRUE	Stress at Max. Load (ksi) Eng. (UTS)	TRUE	Strain at Max. Load Eng.		TRUE	True Strain at Failure	Power Law (s = K ε^n) ** K	n
				(c)	(d)	(e)			(h)	(i)	(j)	(j)
70	10000	(a)	72	72.5	113.9	131.0	(f)	0.15	0.14	0.385	193.8	0.199
212	9530	(a)	57	57.3	104.2	114.6	(g)	0.1	0.10	0.247	206.2	0.250
400	8900	(a)	52	52.3	58.8	62.3	(g)	0.06	0.06	0.157	77.4	0.076
500	8100	(b)	34	34.1	43.8	46.0	(f)	0.05	0.05	0.166	66.3	0.121
600	6700	(b)	16	16.0	33.3	35.3	(f)	0.06	0.06	0.223	71.2	0.247
700	6300	(b)	10	10.0	15.5	16.4	(f)	0.06	0.06	0.378	24.3	0.137
800	5900	(b)	4	4.0	5	5.3	(f)	0.05	0.05	0.61	6.4	0.063
900	5400	(b)	2.1	2.1								
1000	4900	(b)	2	2.0								

* Average value from 70 F to given temperature.
** This correlation uses true stress and true strain.
(...) - Letters refer to notes on the next page describing the source of each property.

True Stress - True Strain Curve data: *

70 F		212 F		400 F		600 F		800 F	
Strain	Stress (ksi)	Strain	Stress (ksi)	Strain	Stress (ksi)	Strain	Stress (ksi)	Strain	Stress (ksi)
0	0	0	0	0	0	0	0	0	0
0.0073	72.5	0.0060	57.3	0.0059	52.3	0.0024	16	0.0007	4
0.02	89.0	0.02	77.6	0.02	57.5	0.02	27.1	0.02	5.0
0.05	106.8	0.05	97.5	0.05	61.6	0.05	34.0	0.05	5.3
0.10	122.6	0.10	116.0	0.10	65.0	0.10	40.3	0.10	5.5
0.20	140.7	0.20	137.9	0.16	67.2	0.20	47.8	0.20	5.7
0.30	152.5	0.25	145.4			0.22	49.1	0.30	5.9
0.39	160.3							0.50	6.1
								0.61	6.2
(k)	(k)	(k)	(k)	(k)	(k)	(k)	(k)	(k)	(k)

* For temperatures in between those given, use linear interpolation.

Source Notes for Table 5 Properties:

(a) Data Sheet 14 Entry 3 (DS 14 E 3)

(b) Average ratio of irradiated yield to unirradiated yield for 70 - 400 F is 1.6 - this ratio was applied to higher temp. unirradiated yield strength. At 500 F, the result is consistent with trend from 1100 irradiated vs 6061 irradiated. At 600 - 700, the results are conservative (lower) compared to 1100 irradiated vs 6061 irradiated trend.

(c) Calculated from eng. value: $\sigma = s_y * (1 + s_y/E)$

(d) DS 14 E 2 Table 9

(e) Calculated from eng. value: $\sigma = s_{UTS} * (1 + e_{UTS})$

(f) Average ratio of 1100 irradiated to 6061 irradiated at 200 - 400 F values is 0.6 - this ratio was applied to 70 and 500 - 700 F irradiated 1100 values

(g) The ratio between total strain and uniform strain from DS 14 E 3 Figure 4 was used to calculate a uniform strain from the failure strain (converted from true strain). This approach provides a better trend to the other values than using the DS 14 E 3 values directly.

(h) Calculated from eng. value: $\varepsilon = \ln(1 + e)$

(i) DS 14 E 2 Table 9, converted to true strain

(j) Values from fit to true yield stress and true stress at max. load, with corresponding true strains

(k) First two values define elastic range; remaining values define plastic range, up to failure strain

Figure 1. True Stress - True Strain Curves for Unirradiated Al 1100

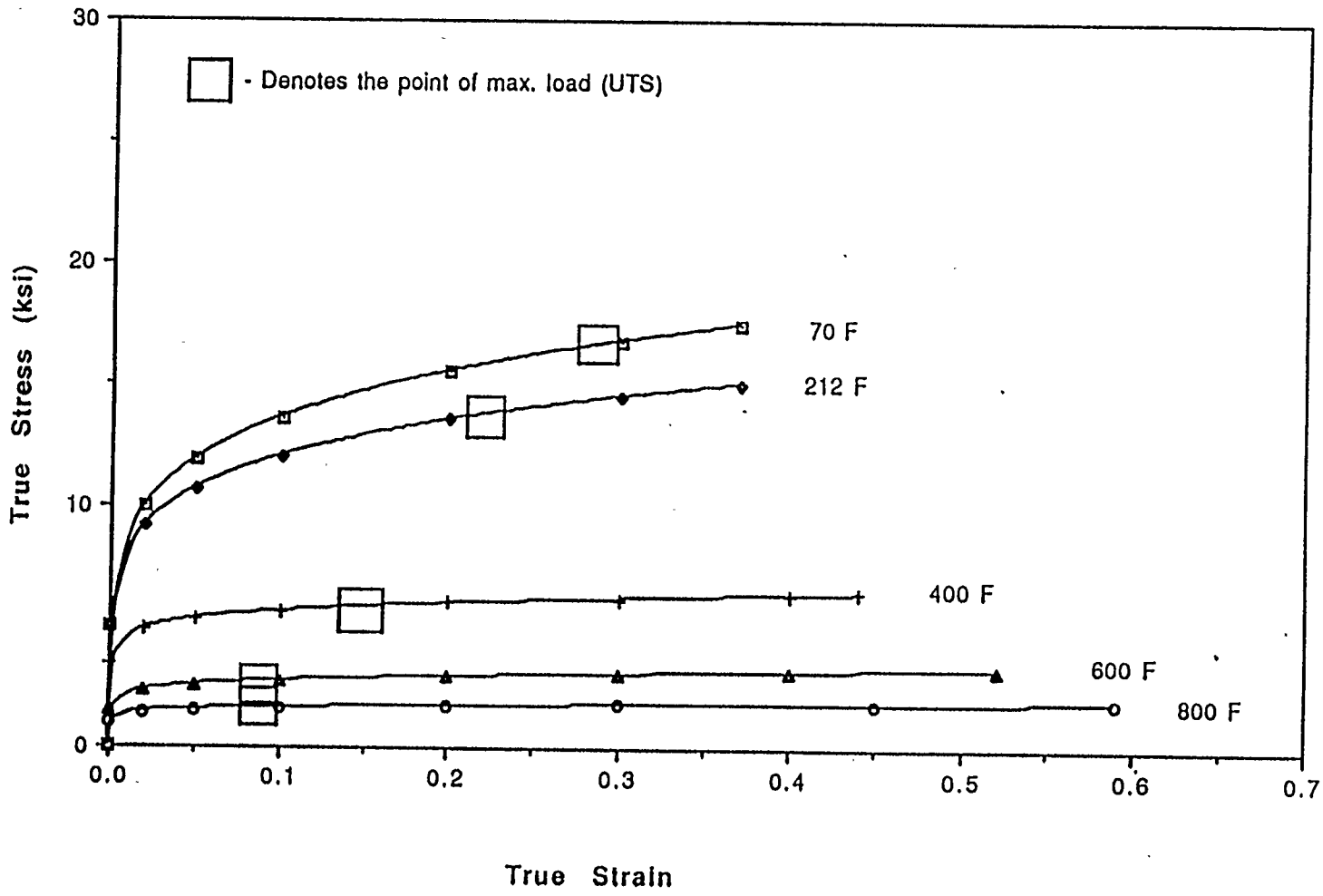

Figure 2. True Stress - True Strain Curves for Irradiated Al 1100

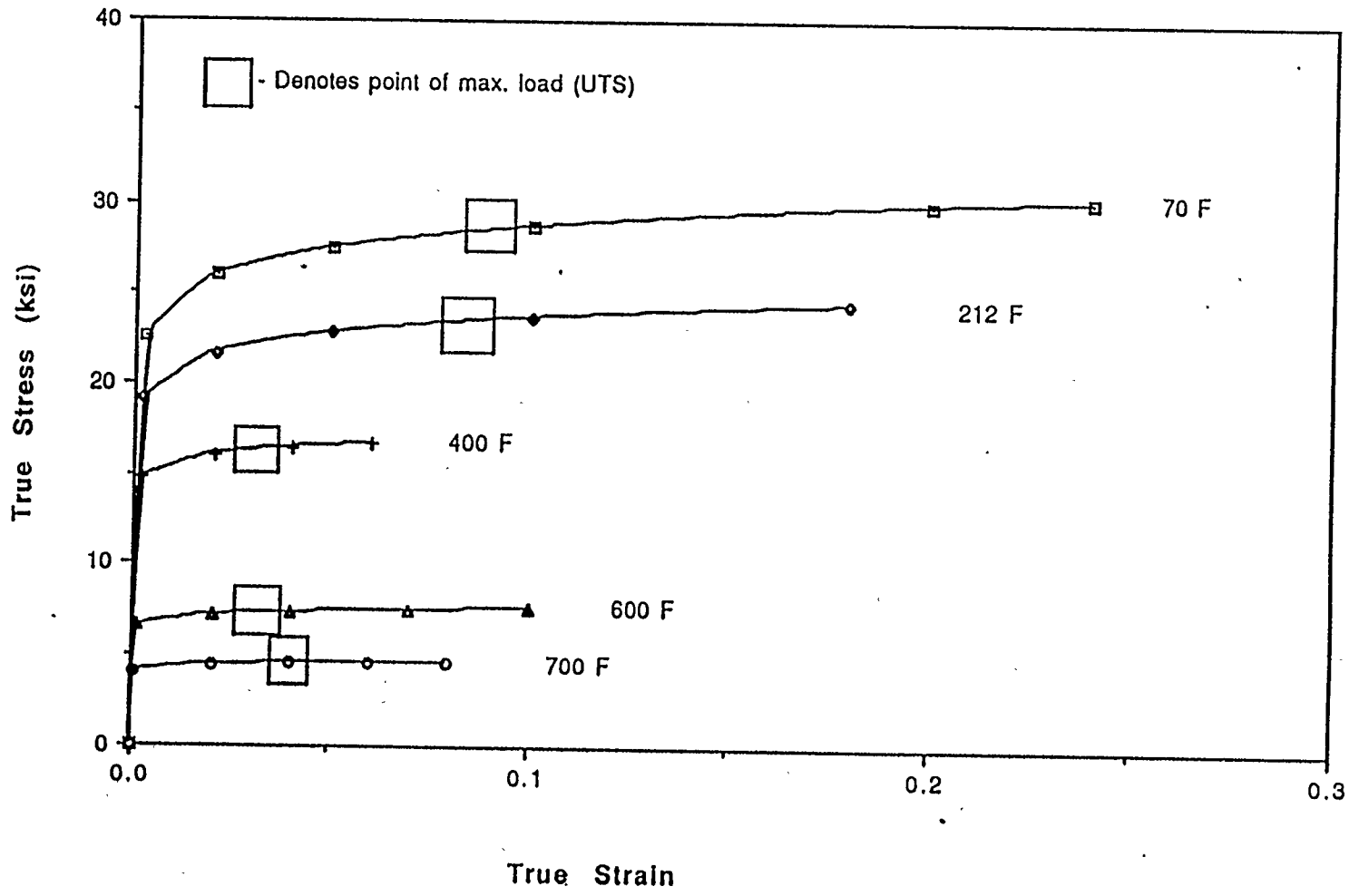

Figure 3. True Stress - True Strain Curves for Unirradiated Al 6061

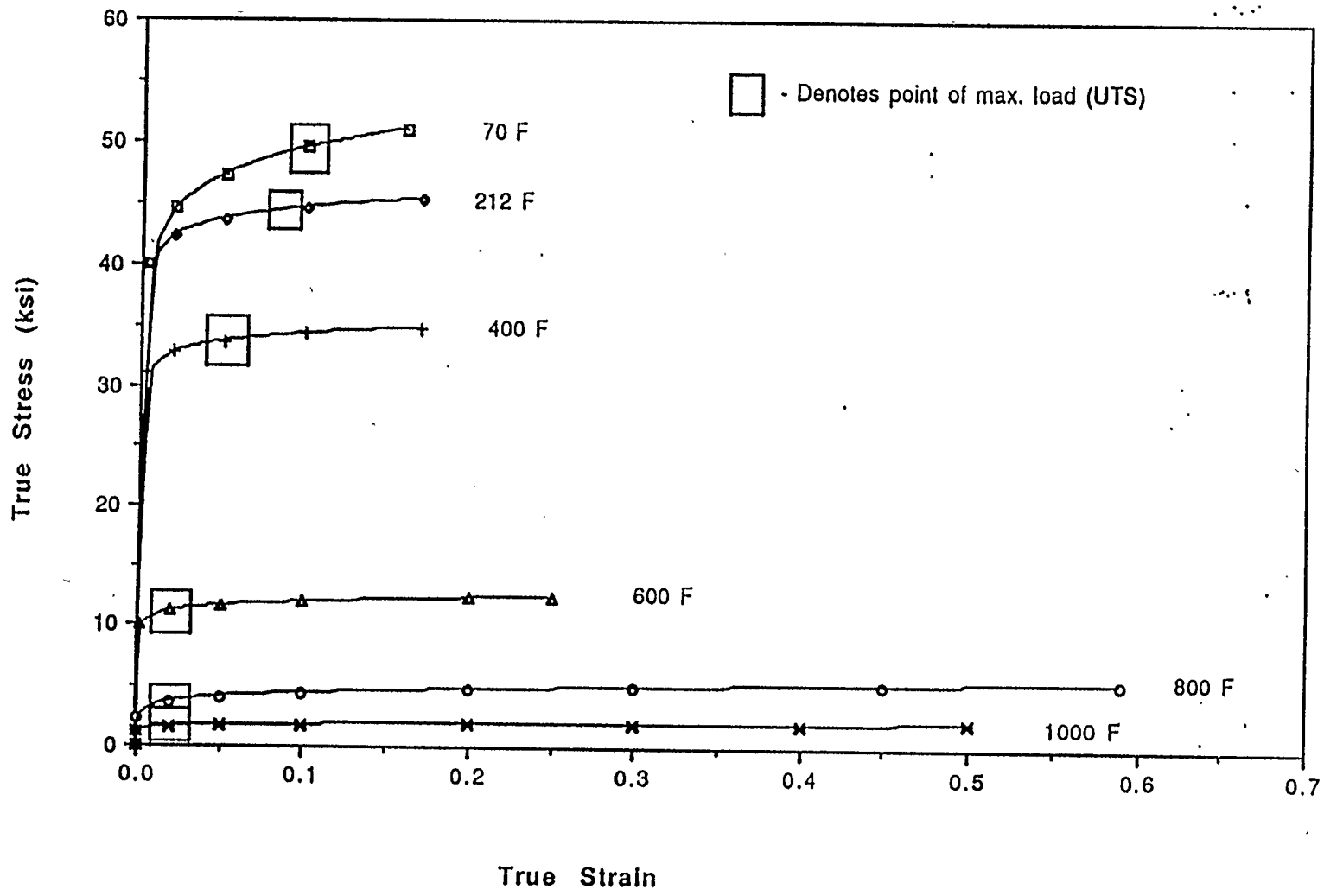

Figure 4. True Stress - True Strain Curves for Irradiated Al 6061

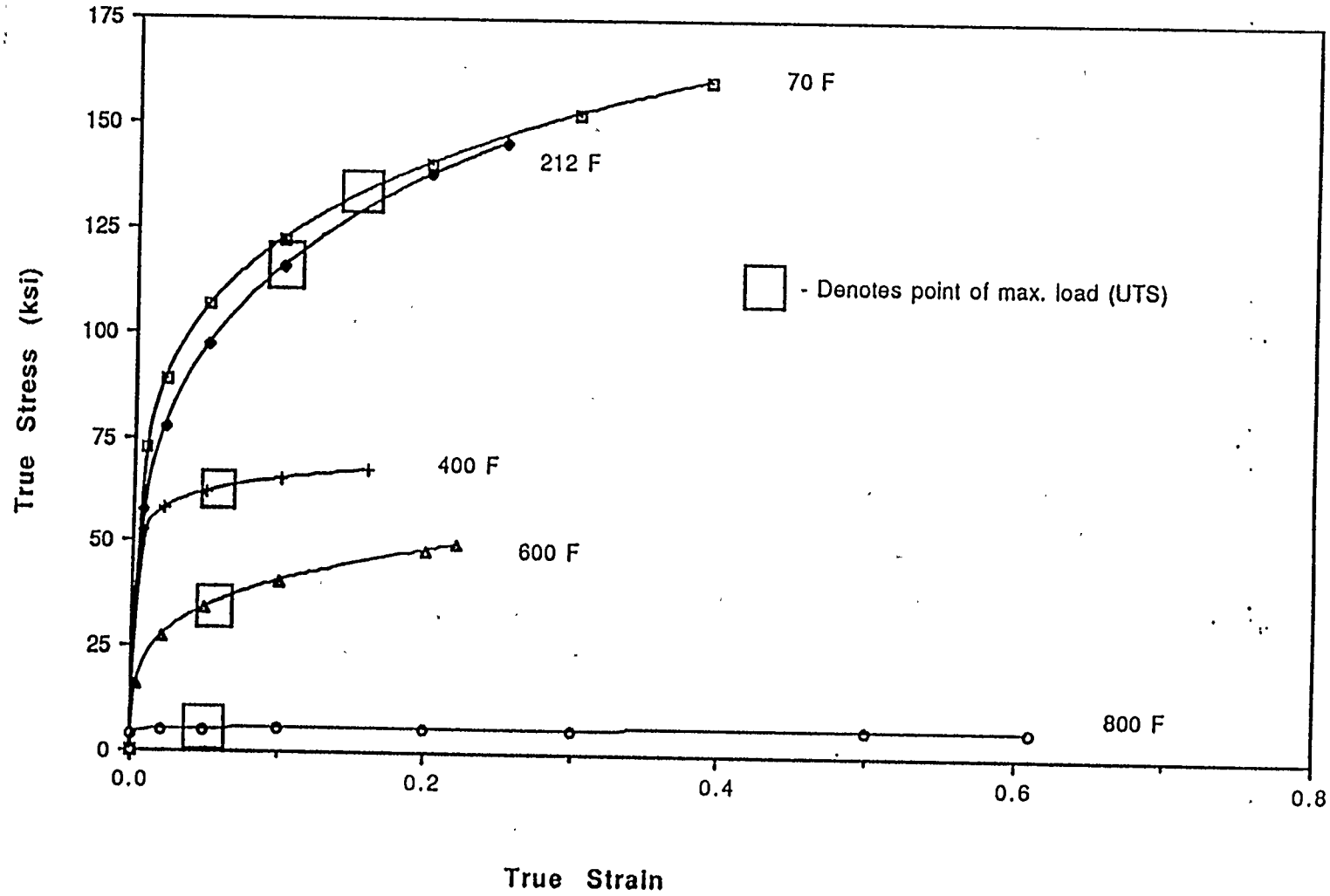

M96009642